THE JOURNAL OF PHYSICAL CHEMISTRY Letters

Letter

Cite This: J. Phys. Chem. Lett. 2019, 10, 1251−1258

pubs.acs.org/JPCL

Optical Gain from Biexcitons in $CsPbBr_3$ Nanocrystals Revealed by Two-dimensional Electronic Spectroscopy

Wei Zhao,[†,‡] Zhengyuan Qin,[‡] Chunfeng Zhang,*[,‡] Guodong Wang,[‡] Xinyu Huang,[‡] Bin Li,[‡] Xingcan Dai,*[,†] and Min Xiao*[,‡,§]

[†]Department of Physics, Tsinghua University, Beijing 100084, China

[‡]National Laboratory of Solid State Microstructures, School of Physics, and Collaborative Innovation Center of Advanced Microstructures, Nanjing University, Nanjing 210093, China

[§]Department of Physics, University of Arkansas, Fayetteville, Arkansas 72701, United States

Supporting Information

ABSTRACT: Perovskite semiconductor nanocrystals (NCs) exhibit highly efficient optical gain, which is promising for laser applications. However, the intrinsic mechanism of optical gain in perovskite NCs, particularly whether more than one exciton per NCs is required, remains poorly understood. Here, we use two-dimensional electronic spectroscopy to resonantly probe the interplay between near-band-edge transitions during the buildup of optical gain in $CsPbBr_3$ NCs. We find compelling evidence to conclude that optical gain in $CsPbBr_3$ NCs is generated through stimulated emission from strongly interacting biexcitons. The threshold is largely determined by the competition between stimulated emission from biexcitons and excited-state absorption from single exciton to biexciton states. The findings in this work may guide future explorations of NC materials with low-threshold optical gain.

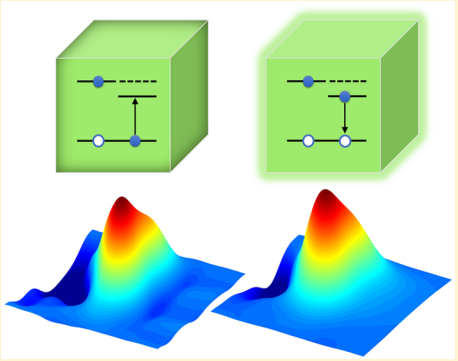

Perovskite semiconductor nanocrystals (NCs) have recently emerged as an important class of materials with inherent properties that are attractive for a wide range of optoelectronic applications.[1−14] For example, all-inorganic cesium lead halide perovskite ($CsPbX_3$) NCs exhibit narrow photoluminescence (PL) emission with a high quantum yield.[1,5] Remarkably, the PL wavelengths can be tuned to cover the visible and near-infrared regions by composition engineering and size control through cost-effective solution-based procedures,[15−17] making perovskite NCs ideal for potential applications in next-generation display devices.[1,18−21] Of more interest, the high modal optical gain demonstrated in a wide range of perovskite semiconductor NCs indicates their great promises for optical amplification and laser applications.[22−24] The solution processability of such NCs enables their implantation into various optical microresonators for on-chip integration. A variety of NC lasers have been demonstrated, such as whispering-gallery-mode lasers,[1,23] vertical cavity surface emitting lasers,[25,26] and random lasers,[1,27] upon linear and nonlinear optical pumping.[23,27−29]

Despite remarkable progress in the development of NC laser devices, the intrinsic mechanism underlying the optical gain in perovskite NCs remains poorly understood. It is under debate whether more than one exciton per NCs is necessary for optical gain generation in perovskite NCs,[1,23,24,30,31] which is theoretically determined by the degeneracies of the involved electron and hole levels. This issue has been intensively surveyed for CdSe NCs by experimentally measuring the threshold of the average number of excitons per NC ($\langle N_g \rangle$).[32−35] Monoexciton ($|X\rangle$) gain and biexciton ($|XX\rangle$) gain can be distinguished by their threshold values ($\langle N_g \rangle$) of 0.69 and 1.15, respectively (see Figure 1a,b).[35] In addition, the interaction between multiple excitons within a single NC could complicate the physical processes involved in gain generation. Auger recombination induced by multiexciton interaction may shorten the lifetime duration of optical gain. Conversely, the multiexciton interaction may decrease the spectral overlap between the absorption of unexcited NCs and biexciton stimulated emission (SE), leading to a decrease in laser threshold.[35] Power-dependent PL emission and ultrafast transient absorption (TA) spectroscopy has been used to study the gain mechanism of perovskite NCs.[23,24,30,36,37] However, the reported values of laser thresholds are divergently distributed (Figure 1c), making it difficult to assign the exact mechanism of gain generation. The thresholds determined from power-dependent amplified spontaneous emission (ASE) measurements have ranged over 2 orders of magnitude, from 2 to 192 $\mu J\ cm^{-2}$,[1,23,24,28,38−40] which is possibly related to the different reabsorption behavior in diverse samples and/or the experimental errors. Because of the spectral overlap between SE and excited-state absorption

Received: February 23, 2019
Accepted: February 27, 2019
Published: February 27, 2019

DOI: 10.1021/acs.jpclett.9b00524
J. Phys. Chem. Lett. 2019, 10, 1251−1258

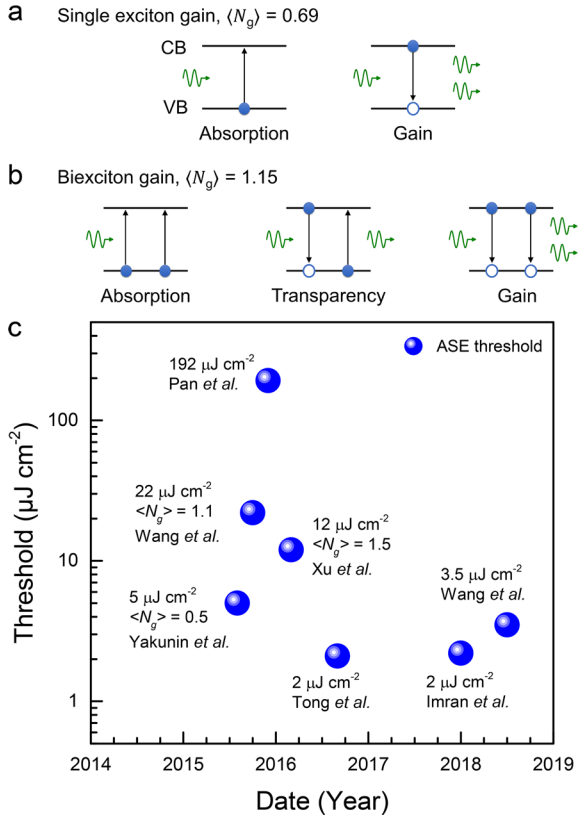

Figure 1. (a, b) Schematic diagram of optical gain mechanisms in semiconductor NCs. In these models, monoexciton and biexciton gains are determined by band-edge states degeneracy factors. (c) ASE thresholds of $CsPbBr_3$ NCs films reported in literature.[1,23,24,28,38−40]

(ESA), it is challenging to directly confirm monoexciton or biexciton gain using TA spectroscopy.[23]

In this work, we study the intrinsic gain mechanism in $CsPbBr_3$ NCs using the two-dimensional electronic spectroscopy (2DES). Different from the conventional time-resolved optical approaches, 2DES can dissect ensembles and overcome the effect of inhomogeneous broadening[41−46] to largely avoid the effects related to different-sized NCs in previous studies. Moreover, 2DES provides information encoding real-time correlations between the energies of states photoexcited and probed states,[41,47−49] enabling direct comparison between resonantly excited band-edge states and hot excitonic states in semiconductors. These advantages enable us to distinguish the dynamics of biexciton states and hot excitonic states during the buildup of optical gain. We clearly observe the characteristics of SE and optical gain generation in the absorptive 2DES spectra of $CsPbBr_3$ NCs. We argue that the optical gain is generated when the biexcitonic SE ($|XX\rangle \rightarrow |X\rangle$) surpasses the losses caused by both ESA of single excitons ($|X\rangle \rightarrow |XX\rangle$) and absorption of unexcited NCs. Theoretical analysis of the power-dependent 2DES results suggests that optical gain in $CsPbBr_3$ NCs involves contributions from strongly interacting biexcitons, which is consistent with the marked spectral red shift of ASE with respect to spontaneous emission from $CsPbBr_3$ NCs.[36] The findings in this work suggest manipulating biexcitonic interaction may be an effective approach to further improve the performance of the lasers based on perovskite NCs.

Synthesis of colloidal $CsPbBr_3$ NCs has previously been described in detail.[23] In brief, Cs_2CO_3 (0.8 g, 99%, Sigma-Aldrich) and oleic acid (OA, 2.5 mL, 90%, Sigma-Aldrich) were dissolved in octadecene (ODE, 30 mL, 90%, Sigma-Aldrich) at 150 °C and then maintained at 100 °C. $PbBr_2$ (0.138 g, 98%, Sigma-Aldrich) was dissolved in ODE (10 mL) at 180 °C with a 1:1 mixture of oleylamine (OLA, 1 mL, 70%, Sigma-Aldrich) and OA (1 mL). The Cs-oleate precursor solution was quickly injected into the lead halide solution. The reaction time was conducted for 5 s before the reaction mixture was placed in an ice−water bath. The purified NCs were dispersed in toluene and then added to an 1 mm thick quartz cuvette. The PL of solution sample centers at 2.44 eV with a full width at half-maximum (fwhm) of ∼101 meV (Figure 2b). Quantum yield of PL emission from the toluene solution sample is above 90%. Time-resolved PL spectrum indicates the emission decay is dominated by an exponential decay component with a lifetime of ∼4 ns (Figure S1, Supporting Information), suggesting that PL emission from the solution sample is mainly caused by the photoexcited neutral excitons. Drop-cast films on quartz substrates were prepared for ASE measurements. Figure 2a shows the sample morphology of the $CsPbBr_3$ NCs characterized by transmission electron microscopy (TEM). The NCs exhibit cubic phase with an average size of 8 nm.

Optical measurements were conducted using a Ti:sapphire regenerative amplifier (Libra, Coherent, 1 kHz) generating laser pulses at 800 nm with a duration of 90 fs. For power-dependent ASE measurements, the frequency doubled beam at 400 nm was used as the excitation source. A spherical lens with a 10 cm focal length was then used to focus the laser beam onto the sample. The edge emission was collected and detected by a fiber spectrometer (USB2000+, Ocean Optics). Our 2DES configuration is based on a pump−probe approach with active phase stabilization.[50] Two homemade noncollinear optical parametric amplifiers (NOPAs) pumped by the regenerative amplifier[51] served as pump and probe beams. The pulses were compressed by chirp mirror pairs, enabling a temporal resolution of better than 20 fs. The spectra of pump and probe beams were configured to cover the absorption and PL emission band of the NCs (Figure 2b), respectively. The pump−probe scheme naturally generates absorptive 2DES spectra. In this work, 2DES spectra were generated by calculating the differential transmission in heterodyne detection (see the Supporting Information for details) to elucidate the information on population occupation in samples. The projection-slice theorem has proved that the projection on the emission axis of the real part of an absorptive 2D spectrum provides equivalent to that of a TA signal at the same delay time (Figure S2, Supporting Information).

We record the PL emission spectra from a $CsPbBr_3$ NC film under different excitation fluences (Figure 2c,d). Optical gain induced ASE spectra are acquired when the excitation exceeds a threshold value of 11 $\mu J\ cm^{-2}$ at 400 nm. The ASE feature appears on the red side of spontaneous emission with an energy shift of about 76 meV, which is similar to the literature results.[1] The red shift of ASE emission from $CsPbBr_3$ NCs is much larger than that from CdSe NCs.[35] In principle, such a spectral shift may be induced by the reabsorption effect due to the partial overlap between the absorption and optical gain spectra. Intuitively, the reabsorption effect plays an important role because the ASE peak locates at the photon energy right below the absorption edge. Nevertheless, recent studies based on temporally and spectrally resolved PL measurements suggest that the red-shifted emission is caused by the radiative

DOI: 10.1021/acs.jpclett.9b00524
J. Phys. Chem. Lett. 2019, 10, 1251−1258

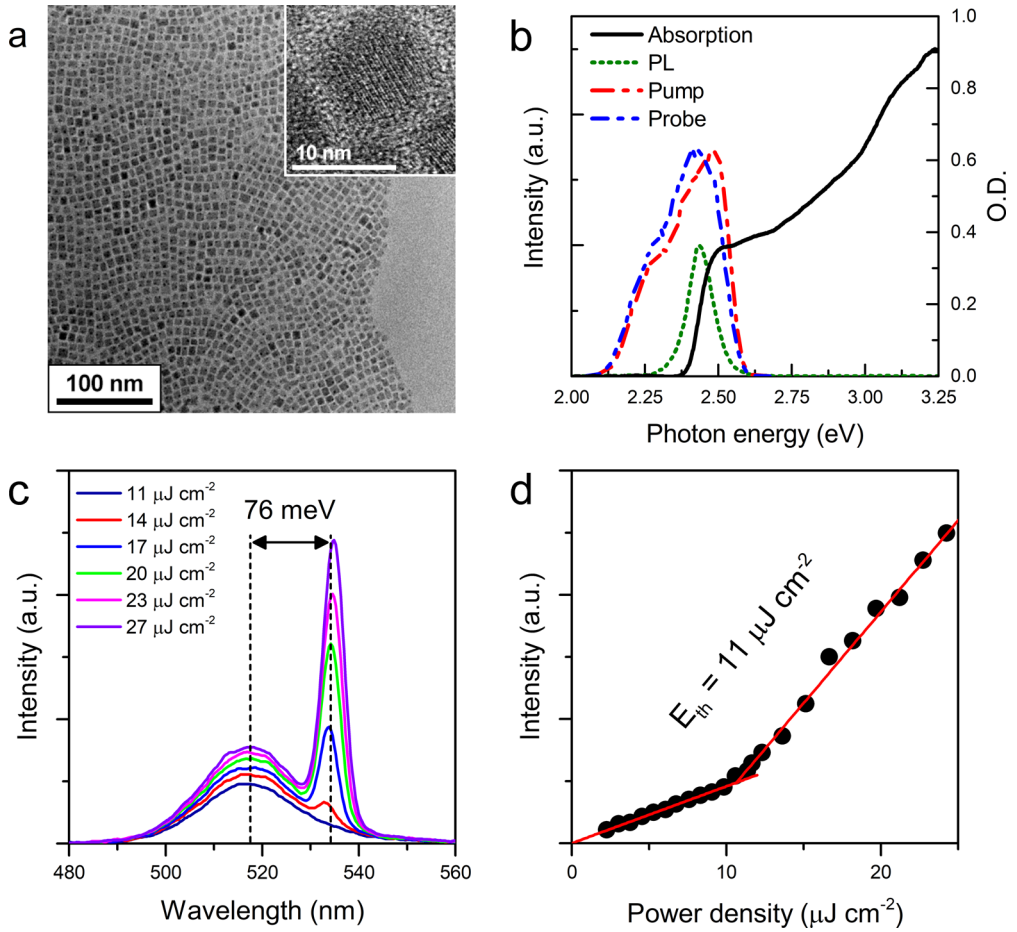

Figure 2. (a) Transmission electron microscopy (TEM) images of cubic $CsPbBr_3$ perovskite NCs. (b) Absorption (black solid) and normalized PL (olive dot) spectra of $CsPbBr_3$ colloidal NCs in solution. Two homemade NOPAs are configured for resonant excitation and detection, serving as the pump and probe beams (red and blue dashed-dotted lines) in 2DES experiments. (c) PL spectra and (d) peak intensities recorded at different excitation fluences from the $CsPbBr_3$ NC film.

recombination of biexcitons with mutual interactions.[36] In this scenario, the red shift is primarily caused by the interaction energy between the excitons.

We perform 2DES measurements on a solution sample of $CsPbBr_3$ NCs at different population time delays and different excitation densities to study the intrinsic mechanism of optical gain in the NCs.[52] Artifact on the time scale <50 fs induced by nonresonant nonlinear optical response from toluene is eliminated from analysis. Compared with TA spectroscopy, 2DES can extract more penetrating information by distinguishing the dynamics of excited states related to different energy excitations. Figure 3 shows the 2DES data recorded at a pump fluence of 10 μJ cm^{-2}. The diagonal main positive peak (at 2.46, 2.46 eV) corresponds to the low lying excitonic transition, which may be contributed by the ground-state bleaching (GSB) and SE of the band-edge transition.

Two major features of ESA, indicated by a circle and square in Figure 3a, appear above and below the diagonal, respectively. The ESA feature above the diagonal (circle) is long-lived (Figure 3c), which can be assigned to the transition from excitons to higher levels. The ESA feature below the diagonal is short-lived with a characteristic lifetime of less than 1 ps (Figure 3d). Such a fast component was assigned to the hot excitons in previous TA studies with a pump wavelength at 400 nm.[23,30,53] In the 2DES spectra, the ESA feature is observed upon excitation resonant with the low-lying excitonic transition (Figure 3a). In this case, the ESA signal mainly originates from relaxed excitons rather than hot excitons. Considering that the photon energy is slightly lower than that of excitons, the short-lived ESA is probably related to the transition from the exciton state ($|X\rangle$) to the biexcitonic state ($|XX\rangle$). Nevertheless, the short lifetime of the ESA remains to be explained. The temporal dynamics reveal that the ESA signal decays while the bleach signal increases after 5 ps (Figure 3d). Such a crossover from negative to positive can be explained if a delayed SE component is considered. If the SE mainly originates from single excitons, the buildup processes of ESA and SE are simultaneous, which cannot explain the crossover process. The delayed rise of the SE signal is consistent with a scenario involving the formation of a biexciton from two independent excitons (Figure 3e). For a single exciton in a NC, optical transitions with energies near the band gap involve the ESA from $|X\rangle$ to $|XX\rangle$ and SE from $|X\rangle$ to the ground state. When a biexciton is formed in a NC, the ESA caused by the transition from $|X\rangle$ to $|XX\rangle$ is eliminated, but the SE caused by the transition from $|XX\rangle$ to $|X\rangle$ states becomes prominent. If some NCs initially absorb two photons, the two independent excitons may be converted to the low-energy bound state,[30] i.e., $|XX\rangle$, leading to the crossover from ESA to the bleaching signal probed at 2.39 eV.

Considering the above model (Figure 3e), we can interpret the entire 2DES data by the global analysis scheme following

DOI: 10.1021/acs.jpclett.9b00524
J. Phys. Chem. Lett. 2019, 10, 1251−1258

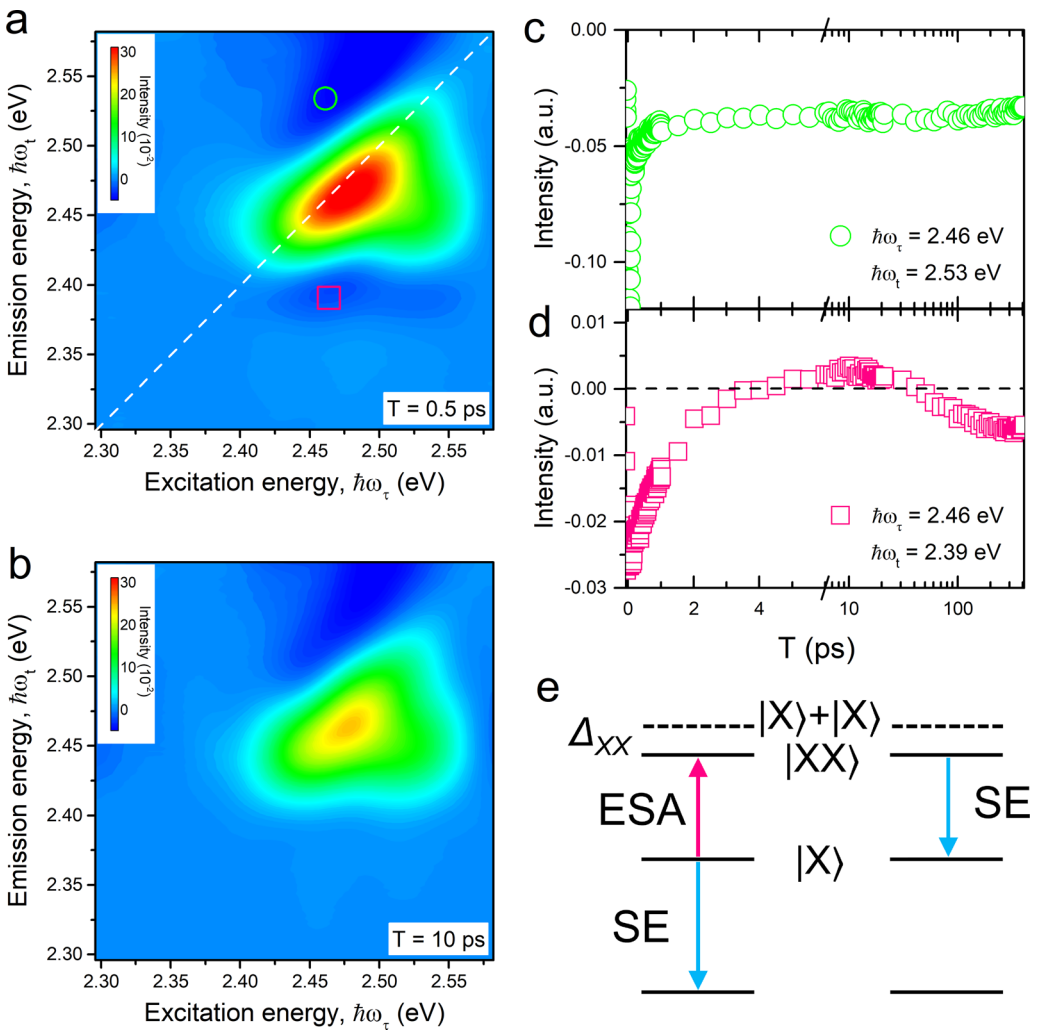

Figure 3. Absorptive 2DES spectra of $CsPbBr_3$ NCs at the population times (a) 0.5 and (b) 10 ps, respectively. The pump fluence is set at 10 μJ cm^{-2}. The major ESA features are indicated by a circle and square in (a). (c, d) Temporal dynamics of the ESA features marked in (a). (e) Schematic diagram of the near-band-edge transitions related to a single exciton |X⟩ (left) and biexciton |XX⟩ (right).

the literature protocol (see the Supporting Information for details).[54,55] The dynamics of 2DES data recorded at 10 μJ cm^{-2} can be reproduced with four decay components with significantly different lifetimes. An ultrafast component with a lifetime of ~100 fs (Figure S3a) is probably caused by the cooling process of hot excitons while the formation of biexciton is observed with a component of ~2 ps (Figure S3b). In comparison with that of biexciton formation, the signal of the ultrafast component (~100 fs) is more pronounced under higher energy excitation. These results explicitly verify the above assignment of the short-lived ESA signal to the transition from |X⟩ to |XX⟩ states with resonant excitation (Figure 3). Moreover, the Auger recombination of biexciton (Figure S3c) and the interband recombination of the single exciton (Figure S3d) are observed as the components with lifetimes of ~80 ps and 4 ns, respectively. The line shape of the biexciton signal becomes broader due to exciton interaction (Figure S3c). The downhill excitation transfer is observed as the lower right features in the signal of the single exciton (Figure S3d).

SE from |XX⟩ to |X⟩ states is observed in the ASE spectral range, which is responsible for the optical gain generation in the NCs (Figure 3, Figure S4). The above analysis implies that optical gain in $CsPbBr_3$ NCs at the red tail of the spectral range is contributed by interacting biexcitons. The spectral shift between the GSB and SE, which is ~80 meV in the 2D spectra, is caused by the biexciton interaction Δ_{XX}. This value is comparable to that observed in the ASE spectrum, supporting the scenario of biexciton gain in $CsPbBr_3$ NCs. The electronic correlations between the biexcitons and the fine structures may be more accurately quantified by double-quantum 2DES,[56,57] which will be a future subject with an upgraded setup.

The above assignment is further supported by power-dependent measurements. Parts a and b of Figure 4 compare the 2D spectra recorded at a population delay of 5 ps with pump fluences of 2 and 25 μJ cm^{-2}, respectively. Upon high-fluence excitation, SE from biexcitonic recombination (Figure 4b) becomes dominant, surpassing the loss caused by ESA of single excitons (Figure 4a). Such competitive behavior is manifested in the power dependences of the signals (Figure 4c). The gain is observed with a superlinear dependence on the incident power when the pump fluence exceeds a certain threshold value. In addition, the dynamics of SE generation strongly depends on fluence (Figure 4d). With increasing pump fluence, the rate of biexciton SE generation becomes much faster as more NCs absorb more than one photon. This

DOI: 10.1021/acs.jpclett.9b00524
J. Phys. Chem. Lett. 2019, 10, 1251−1258

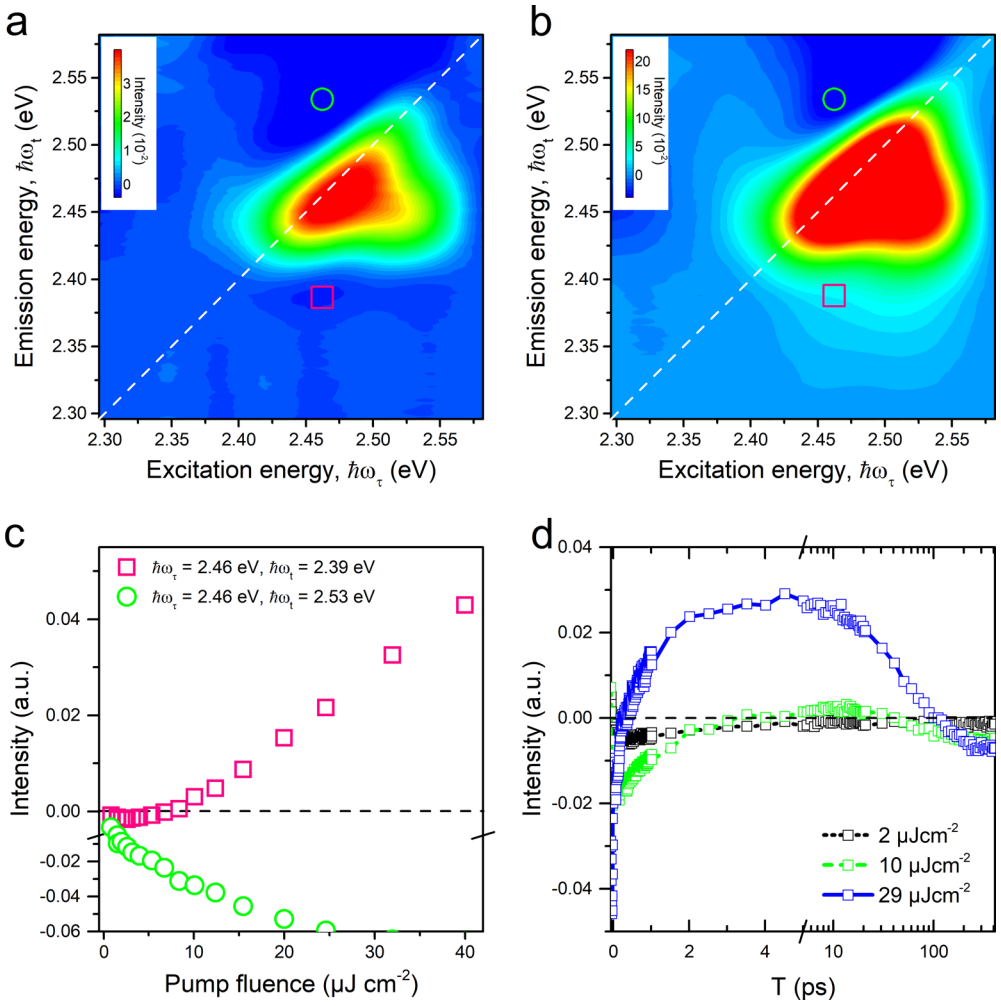

Figure 4. Absorptive 2DES spectra of $CsPbBr_3$ NCs recorded at a population time of 5 ps under pumping with fluences of 2 (a) and 25 μJ cm^{-2} (b), respectively. (c) Pump-fluence-dependent 2DES signals recorded at the excitation and emission photon energies indicated in (a). (d) Dynamics of the 2D signal recorded with excitation at 2.46 eV and emission at 2.39 eV showing the SE buildup under excitations at different fluences.

fluence-dependent behavior supports the presence of multi-exciton interaction during optical generation.

To obtain more insight into the gain mechanism, we compare the experimental data with different models considering optical gain generated from single and multiple excitons. We use the Poisson distribution to describe the photon absorption process in the NCs. With this assumption, the pump-induced change in the probe absorption ($\Delta\alpha$) can be quantitatively calculated (see the details in the Supporting Information). Optical gain is achieved when $-\Delta\alpha > \alpha_0$. Figure 5 compares the experimental data with the models considering gains from a single exciton, biexciton, and biexciton with strong interaction, respectively (Figure 5).[35] The distinction in a monoexciton or biexciton gain is determined by the degeneracy of band-edge states in NCs (Figure 1a,b). The single exciton gain reaches the threshold when $\langle N_g \rangle$ is 0.69, whereas the threshold for a typical biexciton gain with 2-fold degeneracy is $\langle N_g \rangle$ = 1.15.

To minimize the effect of errors in quantifying the threshold, we compare the data on a scale of $\langle N \rangle / \langle N_g \rangle$. As shown in Figure 5, neither the monoexciton model nor the biexciton model can reproduce the power-dependent results obtained for the $CsPbBr_3$ NCs. This is probably caused by the attractive Coulomb interaction energy Δ_{XX} in the NCs. Because of the large Δ_{XX}, the optical gain will appear at the shifted spectral range. Although competition from ESA originating from the $|X\rangle$ to $|XX\rangle$ transition increases, the reabsorption by unexcited NCs is effectively suppressed. In the models, we use the ratio of the interaction energy over the line width of the NC emission band ($r = \Delta_{XX}/\Gamma$) to evaluate the magnitude of the biexciton interaction. The larger the r value is, the lower the threshold gain needs. If r is larger than 42%, the threshold $\langle N_g \rangle$ could be less than 1. Theoretically, if r exceeds 76%, the $-\Delta\alpha/\alpha_0$ signal will be negative when $\langle N \rangle$ is small, which readily explains the ESA at the emission energy of 2.39 eV as observed in our experiment. The degeneracy factors in $CsPbX_3$ NCs determined theoretically are $g_e = g_h = 2$.[34] Our experimental data can be fitted with the biexciton gain model using r = 87%. The corresponding value of Δ_{XX} calculated using the PL line width of $CsPbBr_3$ NCs is about 88 meV (Figure 2b). The fitted value is comparable to the peak shift of 76 meV derived from ASE experiments, which is also consistent with the biexciton binding energy of $CsPbBr_3$ NCs measured from time- and spectrally-resolved PL spectra.[36] A similar level of biexciton binding energy was also been observed in $MAPbBr_3$ NCs,[58]

DOI: 10.1021/acs.jpclett.9b00524
J. Phys. Chem. Lett. 2019, 10, 1251−1258

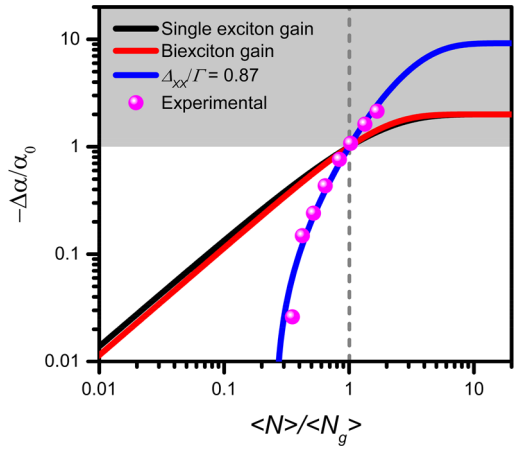

Figure 5. Exciton-density-dependent gain generation. The solid lines show the simulated exciton-density dependences of $-\Delta\alpha/\alpha_0$ using three different models. Optical gain is achieved when $-\Delta\alpha/\alpha_0$ exceeds 1 (region inside the gray rectangle). The horizontal axis is normalized as $\langle N\rangle/\langle N_g\rangle$, where $\langle N_g\rangle$ indicates the gain threshold. Different gain mechanisms show different growth rates. If a large exciton−exciton interaction energy Δ_{XX} is included in the model of biexciton gain, $-\Delta\alpha/\alpha_0$ at the shifted position (blue solid line) grows at a fairly high rate. Meanwhile, the $-\Delta\alpha/\alpha_0$ is negative at small $\langle N\rangle$ region and appears as ESA in our experimental results. The magenta circles indicate the signal data (2.46 eV, 2.39 eV) obtained in our power-dependent 2DES measurements.

suggesting that strong biexcitonic interactions are probably a common characteristic of the lead halide perovskite NCs.

We have conducted 2DES experiments on $CsPbBr_3$ NCs to study their optical gain mechanism. 2DES allows us to study the interplay between different transitions of near band-edge states during the generation of optical gain. We have shown that the generation of optical gain in $CsPbBr_3$ NCs can be described by considering biexcitons with strong interactions. The lasing threshold can be reduced to a remarkably low level ($\langle N_g\rangle < 1$) benefiting from the spectral shift caused by the mutual interaction between excitons. Together with the extrinsic loss, the competition between SE from biexcitons ($|XX\rangle \rightarrow |X\rangle$) and ESA from single exciton to biexciton states ($|X\rangle \rightarrow |XX\rangle$) primarily sets the threshold value. These findings may be used to guide the design and synthesis of perovskite NCs with low-threshold optical gain. The mutual interaction between biexcitons in NCs depends on the size and shape of the NCs, which can be manipulated to further lower the lasing threshold. The spectral coverage between SE and absorption is shown to be critical for gain generation, implying that core/shell engineering, which has been well established for CdSe NCs,[32,33,59] may be a valuable strategy to optimize the laser performance of perovskite NCs. Moreover, by changing the ESA from the single exciton to biexciton state ($|X\rangle \rightarrow |XX\rangle$) in charged NCs, the trion gain may be effective to markedly lower the excitation density required for gain generation.[40] These approaches may facilitate the use of perovskite NCs in continuous-wave pumped and electrically pumped lasers.

■ ASSOCIATED CONTENT

Supporting Information

The Supporting Information is available free of charge on the ACS Publications website at DOI: 10.1021/acs.jpclett.9b00524.

Experimental details, global analysis of entire 2DES data, theoretical models of gain mechanisms, fitting details, and additional 2DES results for $CsPbBr_3$ NCs (PL spectrum, absorption maps and spectra, decay components, gain generation diagram and mechanism models) (PDF)

■ AUTHOR INFORMATION

Corresponding Authors

*E-mail: cfzhang@nju.edu.cn.
*E-mail: xingcandai@mail.tsinghua.edu.cn;.
*E-mail: mxiao@uark.edu.

ORCID

Chunfeng Zhang: 0000-0001-9030-5606

Notes

The authors declare no competing financial interest.

■ ACKNOWLEDGMENTS

This work was supported by the National Key R&D Program of China (2018YFA0209100 and 2017YFA0303703), the National Natural Science Foundation of China (21873047, 91850105, 11574140, 91833305, 11621091, and 11474178), Jiangsu Provincial Funds for Distinguished Young Scientists (BK20160019), the Priority Academic Program Development of Jiangsu Higher Education Institutions (PAPD), and the Fundamental Research Funds for the Central Universities. C.Z. acknowledges financial support from the Tang Scholar program. The authors acknowledge Dr. Xuewei Wu for his technical assistance.

■ REFERENCES

(1) Protesescu, L.; Yakunin, S.; Bodnarchuk, M. I.; Krieg, F.; Caputo, R.; Hendon, C. H.; Yang, R. X.; Walsh, A.; Kovalenko, M. V. Nanocrystals of Cesium Lead Halide Perovskites ($CsPbX_3$, X = Cl, Br, and I): Novel Optoelectronic Materials Showing Bright Emission with Wide Color Gamut. *Nano Lett.* **2015**, *15*, 3692−3696.

(2) Zhang, F.; Zhong, H.; Chen, C.; Wu, X.-g.; Hu, X.; Huang, H.; Han, J.; Zou, B.; Dong, Y. Brightly Luminescent and Color-Tunable Colloidal CH3NH3PbX$_3$ (X = Br, I, Cl) Quantum Dots: Potential Alternatives for Display Technology. *ACS Nano* **2015**, *9*, 4533−4542.

(3) Akkerman, Q. A.; Rainò, G.; Kovalenko, M. V.; Manna, L. Genesis, Challenges and Opportunities for Colloidal Lead Halide Perovskite Nanocrystals. *Nat. Mater.* **2018**, *17*, 394−405.

(4) Kovalenko, M. V.; Protesescu, L.; Bodnarchuk, M. I. Properties and Potential Optoelectronic Applications of Lead Halide Perovskite Nanocrystals. *Science* **2017**, *358*, 745−750.

(5) Di Stasio, F.; Christodoulou, S.; Huo, N.; Konstantatos, G. Near-Unity Photoluminescence Quantum Yield in $CsPbBr_3$ Nanocrystal Solid-State Films via Postsynthesis Treatment with Lead Bromide. *Chem. Mater.* **2017**, *29*, 7663−7667.

(6) Hu, F.; Zhang, H.; Sun, C.; Yin, C.; Lv, B.; Zhang, C.; Yu, W. W.; Wang, X.; Zhang, Y.; Xiao, M. Superior Optical Properties of Perovskite Nanocrystals as Single Photon Emitters. *ACS Nano* **2015**, *9*, 12410−12416.

(7) Swarnkar, A.; Marshall, A. R.; Sanehira, E. M.; Chernomordik, B. D.; Moore, D. T.; Christians, J. A.; Chakrabarti, T.; Luther, J. M. Quantum Dot-Induced Phase Stabilization of alpha-$CsPbI_3$ Perovskite for High-efficiency Photovoltaics. *Science* **2016**, *354*, 92−95.

(8) Chen, Q.; Wu, J.; Ou, X.; Huang, B.; Almutlaq, J.; Zhumekenov, A. A.; Guan, X.; Han, S.; Liang, L.; Yi, Z.; Li, J.; Xie, X.; Wang, Y.; Li, Y.; Fan, D.; Teh, D. B. L.; All, A. H.; Mohammed, O. F.; Bakr, O. M.; Wu, T.; Bettinelli, M.; Yang, H.; Huang, W.; Liu, X. All-inorganic Perovskite Nanocrystal Scintillators. *Nature* **2018**, *561*, 88.

DOI: 10.1021/acs.jpclett.9b00524
J. Phys. Chem. Lett. 2019, 10, 1251−1258

(9) Manser, J. S.; Christians, J. A.; Kamat, P. V. Intriguing Optoelectronic Properties of Metal Halide Perovskites. *Chem. Rev.* **2016**, *116*, 12956−13008.
(10) Sutherland, B. R.; Sargent, E. H. Perovskite photonic sources. *Nat. Photonics* **2016**, *10*, 295−302.
(11) Ning, C.-Z.; Dou, L.; Yang, P. Bandgap Engineering in Semiconductor Alloy Nanomaterials with Widely Tunable Compositions. *Nature Rev. Mater.* **2017**, *2*, 17070.
(12) Zhang, D.; Yu, Y.; Bekenstein, Y.; Wong, A. B.; Alivisatos, A. P.; Yang, P. Ultrathin Colloidal Cesium Lead Halide Perovskite Nanowires. *J. Am. Chem. Soc.* **2016**, *138*, 13155−13158.
(13) Yin, C.; Chen, L.; Song, N.; Lv, Y.; Hu, F.; Sun, C.; Yu, W. W.; Zhang, C.; Wang, X.; Zhang, Y.; Xiao, M. Bright-Exciton Fine-Structure Splittings in Single Perovskite Nanocrystals. *Phys. Rev. Lett.* **2017**, *119*, 026401.
(14) Chen, L.; Li, B.; Zhang, C.; Huang, X.; Wang, X.; Xiao, M. Composition-Dependent Energy Splitting between Bright and Dark Excitons in Lead Halide Perovskite Nanocrystals. *Nano Lett.* **2018**, *18*, 2074−2080.
(15) Nedelcu, G.; Protesescu, L.; Yakunin, S.; Bodnarchuk, M. I.; Grotevent, M. J.; Kovalenko, M. V. Fast Anion-Exchange in Highly Luminescent Nanocrystals of Cesium Lead Halide Perovskites (CsPbX3, X = Cl, Br, I). *Nano Lett.* **2015**, *15*, 5635−5640.
(16) Parobek, D.; Dong, Y.; Qiao, T.; Rossi, D.; Son, D. H. Photoinduced Anion Exchange in Cesium Lead Halide Perovskite Nanocrystals. *J. Am. Chem. Soc.* **2017**, *139*, 4358−4361.
(17) Protesescu, L.; Yakunin, S.; Kumar, S.; Bär, J.; Bertolotti, F.; Masciocchi, N.; Guagliardi, A.; Grotevent, M.; Shorubalko, I.; Bodnarchuk, M. I.; Shih, C.-J.; Kovalenko, M. V. Dismantling the "Red Wall" of Colloidal Perovskites: Highly Luminescent Formamidinium and Formamidinium−Cesium Lead Iodide Nanocrystals. *ACS Nano* **2017**, *11*, 3119−3134.
(18) Quan, L. N.; Quintero-Bermudez, R.; Voznyy, O.; Walters, G.; Jain, A.; Fan, J. Z.; Zheng, X.; Yang, Z.; Sargent, E. H. Highly Emissive Green Perovskite Nanocrystals in a Solid State Crystalline Matrix. *Adv. Mater.* **2017**, *29*, 1605945.
(19) Pan, J.; Shang, Y.; Yin, J.; De Bastiani, M.; Peng, W.; Dursun, I.; Sinatra, L.; El-Zohry, A. M.; Hedhili, M. N.; Emwas, A.-H.; Mohammed, O. F.; Ning, Z.; Bakr, O. M. Bidentate Ligand-Passivated CsPbI3 Perovskite Nanocrystals for Stable Near-Unity Photoluminescence Quantum Yield and Efficient Red Light-Emitting Diodes. *J. Am. Chem. Soc.* **2018**, *140*, 562−565.
(20) Zhang, X.; Sun, C.; Zhang, Y.; Wu, H.; Ji, C.; Chuai, Y.; Wang, P.; Wen, S.; Zhang, C.; Yu, W. W. Bright Perovskite Nanocrystal Films for Efficient Light-Emitting Devices. *J. Phys. Chem. Lett.* **2016**, *7*, 4602−4610.
(21) Song, J.; Li, J.; Li, X.; Xu, L.; Dong, Y.; Zeng, H. Quantum Dot Light-Emitting Diodes Based on Inorganic Perovskite Cesium Lead Halides ($CsPbX_3$). *Adv. Mater.* **2015**, *27*, 7162−7167.
(22) Yakunin, S.; Protesescu, L.; Krieg, F.; Bodnarchuk, M. I.; Nedelcu, G.; Humer, M.; De Luca, G.; Fiebig, M.; Heiss, W.; Kovalenko, M. V. Low-threshold Amplified Spontaneous Emission and Lasing from Colloidal Nanocrystals of Caesium Lead Halide Perovskites. *Nat. Commun.* **2015**, *6*, 8056−8063.
(23) Xu, Y.; Chen, Q.; Zhang, C.; Wang, R.; Wu, H.; Zhang, X.; Xing, G.; Yu, W. W.; Wang, X.; Zhang, Y.; Xiao, M. Two-Photon-Pumped Perovskite Semiconductor Nanocrystal Lasers. *J. Am. Chem. Soc.* **2016**, *138*, 3761−3768.
(24) Wang, Y.; Li, X.; Song, J.; Xiao, L.; Zeng, H.; Sun, H. All-Inorganic Colloidal Perovskite Quantum Dots: A New Class of Lasing Materials with Favorable Characteristics. *Adv. Mater.* **2015**, *27*, 7101.
(25) Wang, Y.; Li, X.; Nalla, V.; Zeng, H.; Sun, H. Solution-Processed Low Threshold Vertical Cavity Surface Emitting Lasers from All-Inorganic Perovskite Nanocrystals. *Adv. Funct. Mater.* **2017**, *27*, 1605088.
(26) Huang, C.-Y.; Zou, C.; Mao, C.; Corp, K. L.; Yao, Y.-C.; Lee, Y.-J.; Schlenker, C. W.; Jen, A. K. Y.; Lin, L. Y. $CsPbBr_3$ Perovskite Quantum Dot Vertical Cavity Lasers with Low Threshold and High Stability. *ACS Photonics* **2017**, *4*, 2281−2289.
(27) Yuan, S.; Chen, D.; Li, X.; Zhong, J.; Xu, X. In Situ Crystallization Synthesis of $CsPbBr_3$ Perovskite Quantum Dot-Embedded Glasses with Improved Stability for Solid-State Lighting and Random Upconverted Lasing. *ACS Appl. Mater. Interfaces* **2018**, *10*, 18918−18926.
(28) Pan, J.; Sarmah, S. P.; Murali, B.; Dursun, I.; Peng, W.; Parida, M. R.; Liu, J.; Sinatra, L.; Alyami, N.; Zhao, C.; Alarousu, E.; Ng, T. K.; Ooi, B. S.; Bakr, O. M.; Mohammed, O. F. Air-Stable Surface-Passivated Perovskite Quantum Dots for Ultra-Robust, Single- and Two-Photon-Induced Amplified Spontaneous Emission. *J. Phys. Chem. Lett.* **2015**, *6*, 5027−5033.
(29) Wang, Y.; Li, X.; Zhao, X.; Xiao, L.; Zeng, H.; Sun, H. Nonlinear Absorption and Low-Threshold Multiphoton Pumped Stimulated Emission from All-Inorganic Perovskite Nanocrystals. *Nano Lett.* **2016**, *16*, 448−53.
(30) Yumoto, G.; Tahara, H.; Kawawaki, T.; Saruyama, M.; Sato, R.; Teranishi, T.; Kanemitsu, Y. Hot Biexciton Effect on Optical Gain in CsPbI3 Perovskite Nanocrystals. *J. Phys. Chem. Lett.* **2018**, *9*, 2222−2228.
(31) Nagamine, G.; Rocha, J. O.; Bonato, L. G.; Nogueira, A. F.; Zaharieva, Z.; Watt, A. A. R.; de Brito Cruz, C. H.; Padilha, L. A. Two-Photon Absorption and Two-Photon-Induced Gain in Perovskite Quantum Dots. *J. Phys. Chem. Lett.* **2018**, *9*, 3478−3484.
(32) Dang, C.; Lee, J.; Breen, C.; Steckel, J. S.; Coe-Sullivan, S.; Nurmikko, A. Red, Green and Blue Lasing Enabled by Single-exciton Gain in Colloidal Quantum Dot Films. *Nat. Nanotechnol.* **2012**, *7*, 335.
(33) Klimov, V. I.; Ivanov, S. A.; Nanda, J.; Achermann, M.; Bezel, I.; McGuire, J. A.; Piryatinski, A. Single-Exciton Optical Gain in Semiconductor Nanocrystals. *Nature* **2007**, *447*, 441−446.
(34) Makarov, N. S.; Guo, S.; Isaienko, O.; Liu, W.; Robel, I.; Klimov, V. I. Spectral and Dynamical Properties of Single Excitons, Biexcitons, and Trions in Cesium−Lead-Halide Perovskite Quantum Dots. *Nano Lett.* **2016**, *16*, 2349−2362.
(35) Wu, K.; Park, Y.-S.; Lim, J.; Klimov, V. I. Towards Zero-Threshold Optical Gain Using Charged Semiconductor Quantum Dots. *Nat. Nanotechnol.* **2017**, *12*, 1140−1147.
(36) Castañeda, J. A.; Nagamine, G.; Yassitepe, E.; Bonato, L. G.; Voznyy, O.; Hoogland, S.; Nogueira, A. F.; Sargent, E. H.; Cruz, C. H. B.; Padilha, L. A. Efficient Biexciton Interaction in Perovskite Quantum Dots Under Weak and Strong Confinement. *ACS Nano* **2016**, *10*, 8603−8609.
(37) Nagamine, G.; Rocha, J. O.; Bonato, L. G.; Nogueira, A. F.; Zaharieva, Z.; Watt, A. A. R.; de Brito Cruz, C. H.; Padilha, L. A. Two-Photon Absorption and Two-Photon-Induced Gain in Perovskite Quantum Dots. *J. Phys. Chem. Lett.* **2018**, *9*, 3478−3484.
(38) Tong, Y.; Bladt, E.; Aygüler Meltem, F.; Manzi, A.; Milowska Karolina, Z.; Hintermayr Verena, A.; Docampo, P.; Bals, S.; Urban Alexander, S.; Polavarapu, L.; Feldmann, J. Highly Luminescent Cesium Lead Halide Perovskite Nanocrystals with Tunable Composition and Thickness by Ultrasonication. *Angew. Chem., Int. Ed.* **2016**, *55*, 13887−13892.
(39) Imran, M.; Caligiuri, V.; Wang, M.; Goldoni, L.; Prato, M.; Krahne, R.; De Trizio, L.; Manna, L. Benzoyl Halides as Alternative Precursors for the Colloidal Synthesis of Lead-Based Halide Perovskite Nanocrystals. *J. Am. Chem. Soc.* **2018**, *140*, 2656−2664.
(40) Wang, Y.; Zhi, M.; Chang, Y.-Q.; Zhang, J.-P.; Chan, Y. Stable, Ultralow Threshold Amplified Spontaneous Emission from $CsPbBr_3$ Nanoparticles Exhibiting Trion Gain. *Nano Lett.* **2018**, *18*, 4976−4984.
(41) Cundiff, S. T.; Zhang, T.; Bristow, A. D.; Karaiskaj, D.; Dai, X. Optical Two-Dimensional Fourier Transform Spectroscopy of Semiconductor Quantum Wells. *Acc. Chem. Res.* **2009**, *42*, 1423−1432.
(42) Moody, G.; Kavir Dass, C.; Hao, K.; Chen, C.-H.; Li, L.-J.; Singh, A.; Tran, K.; Clark, G.; Xu, X.; Berghäuser, G.; Malic, E.; Knorr, A.; Li, X. Intrinsic Homogeneous Linewidth and Broadening Mechanisms of Excitons in Monolayer Transition Metal Dichalcogenides. *Nat. Commun.* **2015**, *6*, 8315−8320.

DOI: 10.1021/acs.jpclett.9b00524
J. Phys. Chem. Lett. 2019, 10, 1251−1258

(43) Seiler, H.; Palato, S.; Sonnichsen, C.; Baker, H.; Kambhampati, P. Seeing Multiexcitons through Sample Inhomogeneity: Band-Edge Biexciton Structure in CdSe Nanocrystals Revealed by Two-Dimensional Electronic Spectroscopy. *Nano Lett.* **2018**, *18*, 2999−3006.
(44) Gellen, T. A.; Lem, J.; Turner, D. B. Probing Homogeneous Line Broadening in CdSe Nanocrystals Using Multidimensional Electronic Spectroscopy. *Nano Lett.* **2017**, *17*, 2809−2815.
(45) Monahan, D. M.; Guo, L.; Lin, J.; Dou, L.; Yang, P.; Fleming, G. R. Room-Temperature Coherent Optical Phonon in 2D Electronic Spectra of $CH_3NH_3PbI_3$ Perovskite as a Possible Cooling Bottleneck. *J. Phys. Chem. Lett.* **2017**, *8*, 3211−3215.
(46) Cassette, E.; Dean, J. C.; Scholes, G. D. Two-Dimensional Visible Spectroscopy For Studying Colloidal Semiconductor Nanocrystals. *Small* **2016**, *12*, 2234−2244.
(47) Brixner, T.; Stenger, J.; Vaswani, H. M.; Cho, M.; Blankenship, R. E.; Fleming, G. R. Two-Dimensional Spectroscopy of Electronic Couplings in Photosynthesis. *Nature* **2005**, *434*, 625−628.
(48) Lewis, K. L. M.; Ogilvie, J. P. Probing Photosynthetic Energy and Charge Transfer with Two-Dimensional Electronic Spectroscopy. *J. Phys. Chem. Lett.* **2012**, *3*, 503−510.
(49) Richter, J. M.; Branchi, F.; Camargo, F. V. d. A.; Zhao, B.; Friend, R. H.; Cerullo, G.; Deschler, F. Ultrafast Carrier Thermalization in Lead Iodide Perovskite Probed with Two-Dimensional Electronic Spectroscopy. *Nat. Commun.* **2017**, *8*, 376.
(50) Zhu, W.; Wang, R.; Zhang, C.; Wang, G.; Liu, Y.; Zhao, W.; Dai, X.; Wang, X.; Cerullo, G.; Cundiff, S.; Xiao, M. Broadband Two-dimensional Electronic Spectroscopy in an Actively Phase Stabilized Pump-Probe Configuration. *Opt. Express* **2017**, *25*, 21115−21126.
(51) Cerullo, G.; Nisoli, M.; Stagira, S.; De Silvestri, S. Sub-8-fs Pulses from an Ultrabroadband Optical Parametric Amplifier in the Visible. *Opt. Lett.* **1998**, *23*, 1283−1285.
(52) Jonas, D. M. Two-Dimensional Femtosecond Spectroscopy. *Annu. Rev. Phys. Chem.* **2003**, *54*, 425−463.
(53) Aneesh, J.; Swarnkar, A.; Kumar Ravi, V.; Sharma, R.; Nag, A.; Adarsh, K. V. Ultrafast Exciton Dynamics in Colloidal $CsPbBr_3$ Perovskite Nanocrystals: Biexciton Effect and Auger Recombination. *J. Phys. Chem. C* **2017**, *121*, 4734−4739.
(54) Righetto, M.; Bolzonello, L.; Volpato, A.; Amoruso, G.; Panniello, A.; Fanizza, E.; Striccoli, M.; Collini, E. Deciphering Hot- and Multi-exciton Dynamics in Core-shell QDs by 2D Electronic Spectroscopies. *Phys. Chem. Chem. Phys.* **2018**, *20*, 18176−18183.
(55) Bakulin, A. A.; Morgan, S. E.; Kehoe, T. B.; Wilson, M. W. B.; Chin, A. W.; Zigmantas, D.; Egorova, D.; Rao, A. Real-time Observation of Multiexcitonic States in Ultrafast Singlet Fission Using Coherent 2D Electronic Spectroscopy. *Nat. Chem.* **2016**, *8*, 16−23.
(56) Kim, J.; Mukamel, S.; Scholes, G. D. Two-Dimensional Electronic Double-Quantum Coherence Spectroscopy. *Acc. Chem. Res.* **2009**, *42*, 1375−1384.
(57) Bristow, A. D.; Karaiskaj, D.; Dai, X.; Zhang, T.; Carlsson, C.; Hagen, K. R.; Jimenez, R.; Cundiff, S. T. A Versatile Ultrastable Platform for Optical Multidimensional Fourier-transform Spectroscopy. *Rev. Sci. Instrum.* **2009**, *80*, 073108.
(58) Veldhuis, S. A.; Tay, Y. K. E.; Bruno, A.; Dintakurti, S. S. H.; Bhaumik, S.; Muduli, S. K.; Li, M.; Mathews, N.; Sum, T. C.; Mhaisalkar, S. G. Benzyl Alcohol-Treated $CH_3NH_3PbBr_3$ Nanocrystals Exhibiting High Luminescence, Stability, and Ultralow Amplified Spontaneous Emission Thresholds. *Nano Lett.* **2017**, *17*, 7424−7432.
(59) Lim, J.; Park, Y.-S.; Klimov, V. I. Optical Gain in Colloidal Quantum Dots Achieved with Direct-Current Electrical Pumping. *Nat. Mater.* **2017**, *17*, 42−49.

DOI: 10.1021/acs.jpclett.9b00524
J. Phys. Chem. Lett. 2019, 10, 1251−1258